

# The ionization toward the high-mass star-forming region NGC 6334 I<sup>★</sup>

Jorge L. Morales Ortiz<sup>1,3</sup>, Cecilia Ceccarelli<sup>1</sup>, Dariusz C. Lis<sup>4</sup>, Luca Olmi<sup>2,3</sup>, René Plume<sup>5</sup>, and Peter Schilke<sup>6</sup>

<sup>1</sup> UJF-Grenoble 1 / CNRS-INSU, Institut de Planétologie et d’Astrophysique de Grenoble (IPAG) UMR 5274, Grenoble, F-38041, France e-mail: jorge.luis379@gmail.com

<sup>2</sup> Osservatorio Astrofisico di Arcetri - INAF, Largo E. Fermi 5, I-50125, Firenze, Italy

<sup>3</sup> University of Puerto Rico, Río Piedras Campus, Physics Department, Box 23343, UPR station, San Juan, Puerto Rico (USA)

<sup>4</sup> California Institute of Technology, Pasadena, CA 91125, USA

<sup>5</sup> Department of Physics and Astronomy, University of Calgary, Calgary, AB T2N 1N4, Canada

<sup>6</sup> I. Physikalisches Institut der Universität zu Köln, Zùlpicher Str. 77, 50937 Köln, Germany

Received; accepted

## ABSTRACT

**Context.** Ionization plays a central role in the gas-phase chemistry of molecular clouds. Since ions are coupled with the magnetic fields, which can in turn counteract the gravitational collapse, it is of paramount importance to measure their abundance in star-forming regions.

**Aims.** We use spectral line observations of the high-mass star-forming region NGC 6334 I to derive the abundance of two of the most abundant molecular ions, HCO<sup>+</sup> and N<sub>2</sub>H<sup>+</sup>, and consequently, the cosmic ray ionization rate. In addition, the line profiles provide information about the kinematics of this region.

**Methods.** We present high-resolution spectral line observations conducted with the HIFI instrument on board the *Herschel Space Observatory* of the rotational transitions with  $J_{\text{up}} \geq 5$  of the molecular species C<sup>17</sup>O, C<sup>18</sup>O, HCO<sup>+</sup>, H<sup>13</sup>CO<sup>+</sup>, and N<sub>2</sub>H<sup>+</sup>.

**Results.** The line profiles display a redshifted asymmetry consistent with a region of expanding gas. We identify two emission components in the spectra, each with a different excitation, associated with the envelope of NGC 6334 I. The physical parameters obtained for the envelope are in agreement with previous models of the radial structure of NGC 6334 I based on submillimeter continuum observations. Based on our new *Herschel*/HIFI observations, combined with the predictions from a chemical model, we derive a cosmic ray ionization rate that is an order of magnitude higher than the canonical value of  $10^{-17} \text{ s}^{-1}$ .

**Conclusions.** We detect an expansion of the envelope surrounding the hot core of NGC 6334 I, which is mainly driven by thermal pressure from the hot ionized gas in the region. The ionization rate is dominated by cosmic rays originating from outside the source, although X-ray emission from the NGC 6334 I core could contribute to the ionization in the inner part of the envelope.

**Key words.** stars: formation – ISM: clouds – ISM: molecules – ISM: cosmic rays – ISM: abundances

## 1. Introduction

High-mass stars form inside molecular clouds, in the densest and coldest regions, and usually do so in groups (e.g., Zinnecker & Yorke 2007; Rivera-Ingraham et al. 2013). Given the involved timescales and luminosities, the original molecular clouds where high-mass stars form are largely altered and even disrupted by the energetic stellar winds and outflows, X-rays and UV photons from the young stars, and  $\geq \text{MeV}$  particles from the explosions of supernovae in their vicinities. The latter are then diffused by magnetic fields in the Galaxy joining the cosmic rays (CRs) that pervade it. But before the information on their original site is cancelled by the diffusion, CRs can be detected in the vicinity where they are accelerated by supernova shocks, because they ionize the gas much deeper than UV photons and X-rays (e.g., Ceccarelli et al. 2011). Specifically, they ionize the H atoms and H<sub>2</sub> molecules of the Interstellar Medium (ISM), creating H<sub>3</sub><sup>+</sup> ions. Since ion-neutral reactions are much faster than neutral-neutral reactions in cold ( $\leq 100 \text{ K}$ ) gas (as the latter have usually activation barriers), the CR ionization is

the starting point of the synthesis of the hundreds of molecules found in cold molecular clouds, or, in other words, of their chemical enrichment.

The first molecular ions created from H<sub>3</sub><sup>+</sup> are HCO<sup>+</sup> and N<sub>2</sub>H<sup>+</sup>, by reactions with CO and N<sub>2</sub> respectively (e.g., Turner 1995). These ions can, therefore, be used to measure the CR ionization rate. For the reasons mentioned above, this is particularly interesting in high-mass star-forming regions, because it provides us with crucial information on the CR formation and, possibly, how it influences the star formation process. Another crucial, but poorly constrained aspect is how deep CRs can penetrate through a molecular cloud (e.g., Padovani et al. 2009). This is predicted to have important consequences in, for example, the accretion through protoplanetary disks and, consequently, in the planet formation process (e.g., Balbus & Hawley 1998; Gammie 1996). So far, only a few constraints exist on the penetration of CRs at H<sub>2</sub> column densities larger than  $\sim 10^{23} \text{ cm}^{-2}$  (Padovani et al. 2013). Such large densities are reached in high-mass protostars and a few other sites of our galaxy, so this is an additional reason for studying the CR ionization rate in high-mass star-forming regions.

In this work, we present new observations of the HCO<sup>+</sup> and N<sub>2</sub>H<sup>+</sup> molecular ions in the direction of a high-mass star-

<sup>★</sup> *Herschel* is an ESA space observatory with science instruments provided by European-led Principal Investigator consortia and with important participation from NASA.

forming region, NGC 6334 I (see §2). The high-resolution spectral line observations were carried out with the HIFI (Heterodyne Instrument for the Far Infrared) instrument on board the *Herschel Space Observatory* (HSO) as part of the CHES (Chemical *H*erschel Surveys of Star-forming regions) *Herschel* key program (Ceccarelli *et al.* 2010). The goal of the program is to obtain unbiased line surveys of several star-forming regions (see for example, Ceccarelli *et al.* 2010; Codella *et al.* 2010; Zernickel *et al.* 2012; Kama *et al.* 2013). In the survey of NGC 6334 I, we detected several  $J_{\text{up}} \geq 6$   $\text{HCO}^+$ ,  $\text{H}^{13}\text{CO}^+$ , and  $\text{N}_2\text{H}^+$  transitions (Zernickel *et al.* 2012). Given the upper level energies  $\geq 80$  K and critical densities  $\geq 10^7 \text{ cm}^{-3}$  of these transitions, the CHES observations allow us to probe the dense and warm gas in this region and, consequently, the CR ionization rate deep inside the NGC 6334 I envelope. To better constrain the origin of the emission and the physical conditions of the emitting gas, we also used the  $\text{C}^{18}\text{O}$  and  $\text{C}^{17}\text{O}$   $J_{\text{up}} \geq 5$  transitions, detected in the CHES survey.

From the *Herschel*/HIFI observations of these molecular tracers ( $\text{C}^{18}\text{O}$ ,  $\text{C}^{17}\text{O}$ ,  $\text{HCO}^+$ ,  $\text{H}^{13}\text{CO}^+$ , and  $\text{N}_2\text{H}^+$ ), we first determine the line parameters of each of the rotational transitions. With these results, and using a non-Local Thermodynamic Equilibrium (LTE) Large Velocity Gradient (LVG) radiative transfer code, we then model the spectral line emission in order to estimate the physical parameters of the emitting gas (temperature, density, source size, and column density). We also estimate the relative abundances of  $\text{HCO}^+$  and  $\text{N}_2\text{H}^+$  by using the results from the LVG analysis. Finally, by comparing the measured  $\text{HCO}^+$  and  $\text{N}_2\text{H}^+$  abundances with those predicted by a chemical model, we derive an estimate of the CR ionization rate across the region.

This paper is thus organized as follows: in Section 2 we review the main characteristics of NGC 6334 I and previous observations relevant to this work. In Section 3 we describe the observations used in this paper. In Section 4 we present the results of the analysis of the observed molecular line spectra. We then discuss the origin of the observed line profiles and emission, providing the gas temperature and densities, the  $\text{HCO}^+$  and  $\text{N}_2\text{H}^+$  abundances, and the derived CR ionization rate in Section 5. Section 6 concludes.

## 2. Source background

NGC 6334 I is a relatively nearby (1.7 kpc; Neckel 1978) high-mass star-forming region, with a total mass of  $\sim 200 M_{\odot}$ , a bolometric luminosity of  $\sim 2.6 \times 10^5 L_{\odot}$ , and a size of  $\sim 1$  pc in diameter (Sandell 2000). It is associated with an ultra compact HII region (de Pree *et al.* 1995), and masers have been detected in OH (Brooks & Whiteoak 2001),  $\text{H}_2\text{O}$  (Migenes *et al.* 1999),  $\text{CH}_3\text{OH}$  (Walsh *et al.* 1998), and  $\text{NH}_3$  (Walsh *et al.* 2007). NGC 6334 I is a so-called hot core, since it possesses the main characteristics of such objects: high temperatures ( $\geq 100$  K), small sizes ( $\lesssim 0.1$  pc), masses ranging from  $\sim 10 - 10^3 M_{\odot}$ , and luminosities larger than  $10^4 L_{\odot}$  (Cesaroni 2005).

The NGC 6334 I region has been studied in considerable detail over the last decades. We summarize here some of the most recent results which are relevant to the present work. The Submillimeter Array (SMA) 1.3 mm continuum emission image toward NGC 6334 I (see Fig. 1 in Hunter *et al.* 2006) shows that the hot core itself consists of four compact condensations located within a region  $\approx 10''$  in diameter. These four sources are denoted as I-SMA1 – 4 in descending order of peak intensity. The I-SMA1 and I-SMA2 sources show rich spectra of molecular transitions, I-SMA3 is associated with an HII region excited

by the NIR source IRS1E, and I-SMA4 shows dust emission but no line emission (Zernickel *et al.* 2012).

Spectral line observations of the  $\text{NH}_3(1,1)$  through (6,6) inversion lines taken with the Australia Telescope Compact Array (ATCA; Beuther *et al.* 2005 & 2007) show two emission peaks associated with the two brightest continuum sources (I-SMA1 and I-SMA2) reported by Hunter *et al.* (2006). The six inversion lines observed by Beuther and co-authors cover a range of upper level energies  $E_{\text{up}}$  from 23 K to 408 K. From the  $\text{NH}_3(5,5)$  and (6,6) lines, Beuther *et al.* (2007) assigned Local Standard of Rest (LSR) velocities of  $-7.6$  and  $-8.1 \text{ km s}^{-1}$ , and  $-7.5$  and  $-8.0 \text{ km s}^{-1}$  for the I-SMA1 and I-SMA2 sources, respectively.

The radial structure of several star-forming cores, including NGC 6334 I, has been studied by Rolffs *et al.* (2011, hereafter R11) through spectral line observations with the Atacama Pathfinder EXperiment (APEX) and submillimeter continuum maps at  $850 \mu\text{m}$  from the APEX Telescope Large Area Survey of the GALaxy (ATLASGAL) taken with LABOCA (Large APEX bolometer Camera). By modeling the source as a centrally heated sphere with a power-law density gradient, these authors first reproduce the radial intensity profile of the continuum emission at  $850 \mu\text{m}$ . Afterwards, they try to reproduce by radiative transfer modeling the spectral line emission of various HCN,  $\text{HCO}^+$  and CO lines, providing the physical structure derived from the continuum analysis as the input parameters. The models indicate that the density varies with radius as  $r^{-1.5}$ , which gives an effective dust temperature of 65 K and a luminosity of  $7.8 \times 10^4 L_{\odot}$  for NGC 6334 I. While the modeling of the radial profiles is consistent with the continuum observations, the authors are only able to explain some of the observed spectral features in the data. Probably, the inconsistencies in the results are due to the simplified source structure of the radiative transfer model and the actual complexity of the internal structure of NGC 6334 I, which was already revealed by the interferometric data from SMA.

Finally, as already mentioned, previous CHES observations of NGC 6334 I have been already reported by Emprechtinger *et al.* (2010, 2013), Lis *et al.* (2010), Ossenkopf *et al.* (2010), van der Wiel *et al.* (2010), and Zernickel *et al.* (2012). The first detection of  $\text{H}_2\text{Cl}^+$ , in the ISM, toward NGC 6334 I was reported by Lis *et al.* (2010).  $\text{H}_2\text{Cl}^+$  was detected in absorption, and these authors report a column density in excess of  $10^{13} \text{ cm}^{-2}$ . HCl is also detected, in emission, at the hot core velocity ( $\sim -6.3 \text{ km s}^{-1}$ ). The CH emission component reported by van der Wiel *et al.* (2010) at a velocity of  $-8.3 \text{ km s}^{-1}$  is consistent with the  $\text{H}_2\text{O}$  hot core emission detected by Emprechtinger *et al.* (2010) at  $-8.2 \text{ km s}^{-1}$ . The spectral line survey of NGC 6334 I by Zernickel *et al.* (2012) identifies a total of 46 molecules, with 31 isotopologues, in a combination of emission and absorption lines. In particular, for the  $\text{HCO}^+$  and  $\text{H}^{13}\text{CO}^+$  lines the authors derive a velocity of  $-7.5 \text{ km s}^{-1}$  and a line width of  $4.7 \text{ km s}^{-1}$ , and a velocity of  $-6.8 \text{ km s}^{-1}$  and a line width of  $4.6 \text{ km s}^{-1}$  for the CO isotopologues. Two components at velocities of  $-6.8$  and  $-9.5 \text{ km s}^{-1}$  and line widths of  $2.5 \text{ km s}^{-1}$  are determined for  $\text{N}_2\text{H}^+$ . The spectral analysis of water isotopologues by Emprechtinger *et al.* (2013) identifies four physical components in the line profiles. The first component, with a velocity of  $-6.4 \text{ km s}^{-1}$  and a line width of  $5.4 \text{ km s}^{-1}$ , corresponds to the envelope of NGC 6334 I. The second component coincides with the LSR velocity of I-SMA2 ( $\sim -8 \text{ km s}^{-1}$ ), and is thus associated with the embedded core. The other two components are associated, respectively, with foreground clouds and a bipolar outflow.

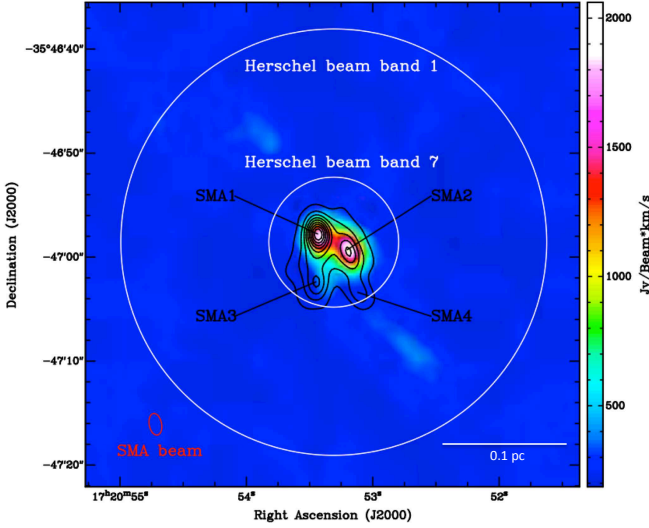


**Fig. 1.** Map of the integrated SMA line intensity over all species reported by Zernickel et al. (2012) toward NGC 6334 I. The black contours represent the continuum emission. The white circles represent the HIFI beam size for band 1 and band 7. Figure from Zernickel et al. (2012).

### 3. Observations

The observations were performed between February 28, and October 14, 2010, with the HIFI instrument on board the *Herschel Space Observatory* in the double beam switch mode (180'' chopper throw). The observed position with *Herschel*/HIFI toward NGC 6334 I ( $\alpha_{2000} = 17^h20^m53.32^s$ ,  $\delta_{2000} = -35^\circ46'58.5''$ ) is located between the I-SMA1 and I-SMA2 sources (Sect. 2). The data have been reduced with the HIPE (Herschel Interactive Processing Environment; Ott 2010) pipeline version 5.1. The spectral resolution of the double sideband (DSB) spectra, which have been observed for 3.5 seconds each, is 1.1 MHz (corresponding to a velocity resolution ranging from 0.3 to 0.6 km s<sup>-1</sup>). The DSB spectra have been observed with a redundancy of eight, which allows the deconvolution and isolation of the single sideband (SSB) spectra (Comito & Schilke 2002). The deconvolved SSB spectra have been exported to the FITS format for subsequent analysis using the IRAM GILDAS package. The spectra shown here are equally weighted averages of the horizontal and vertical polarizations, corrected for the main beam efficiencies (see Sect. 4). In the CHES line survey we detect seven C<sup>18</sup>O lines, five C<sup>17</sup>O lines, seven HCO<sup>+</sup> lines, three H<sup>13</sup>CO<sup>+</sup> lines, and four N<sub>2</sub>H<sup>+</sup> lines. The spatial structure obtained from SMA (Sect. 2) is unresolved by *Herschel* because the beam covers the whole NGC 6334 I region (see Figure 1). The SMA observations thus serve as an auxiliary tool to identify and separate the different components present in the HIFI spectra.

### 4. Results

The spectral line data were analyzed using the IRAM package CLASS. The spectra obtained with HIFI towards NGC 6334 I are shown in Figures 2 to 4. The line parameters, derived from a single Gaussian fit to the spectra, are listed in Table 1. The rotational spectra of C<sup>17</sup>O and N<sub>2</sub>H<sup>+</sup> have a hyperfine structure. However, for the observed lines ( $J_{\text{up}} \geq 5$ ) the hyperfine components are so heavily blended together that, even when determined

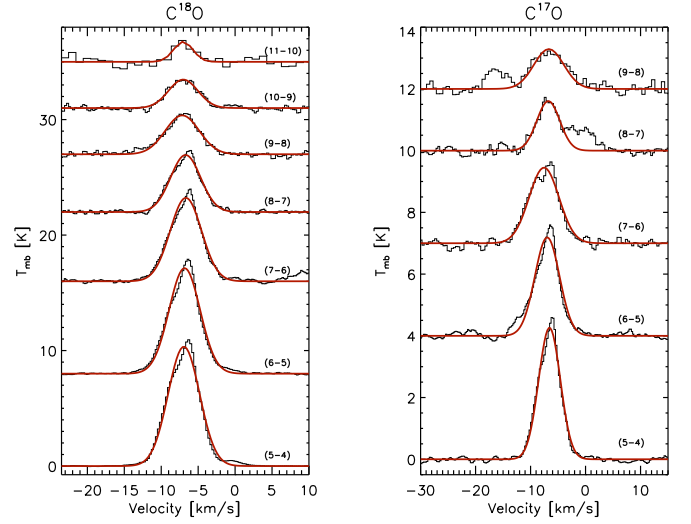


**Fig. 2.** Spectra of the C<sup>18</sup>O and C<sup>17</sup>O lines. The red lines show the Gaussian fits to the spectra.

by a single Gaussian fit, the line width should not be significantly overestimated (Miettinen et al. 2012).

We compute the half-power beamwidth (HPBW) and the main beam efficiency ( $\eta_{\text{mb}}$ ) for HIFI as a function of frequency for each of the detected lines by making linear interpolations from the values listed in Roelfsema et al. (2012). The  $\eta_{\text{mb}}$  values are then used to convert the integrated intensities from the antenna temperature ( $T_{\text{A}}^*$ ) to the main beam temperature ( $T_{\text{mb}}$ ) scale. The RMS of the integrated intensities ( $\sigma_I$ ) is computed as:  $\sigma_I = \sqrt{n \cdot (\sigma_{\text{base}} \cdot \Delta v)^2 + (f \cdot I)^2}$ , where  $\sigma_{\text{base}}$  is the baseline RMS,  $\Delta v$  is the channel width,  $n$  is the number of channels across the line profile,  $I = \int T_{\text{mb}} dv$  is the integrated intensity, and the factor  $f$ , which represents the calibration uncertainty of the HIFI instrument (Roelfsema et al. 2012), is chosen to be 15%.

The observed molecular lines cover upper level energies in the range  $79 \text{ K} \leq E_{\text{up}} \leq 348 \text{ K}$ , thus tracing different physical components within the NGC 6334 I region. The detected C<sup>18</sup>O and HCO<sup>+</sup> lines have similar peak intensities, greater than the peak intensities of the N<sub>2</sub>H<sup>+</sup> lines by a factor ranging from  $\sim 2 - 10$ . Also, the average HCO<sup>+</sup>/H<sup>13</sup>CO<sup>+</sup> line intensity ratio is 18, which is lower than the expected value ( $^{12}\text{C}/^{13}\text{C} \approx 75$ ; Langer & Penzias 1990) by a factor of  $\sim 4$ , thus indicating that the HCO<sup>+</sup> lines are optically thick. The C<sup>18</sup>O lines also suffer from optical depth effects with an average C<sup>18</sup>O/C<sup>17</sup>O ratio of 2.8, which is lower than the expected value of  $^{18}\text{O}/^{17}\text{O} \approx 3.5$  (Penzias 1981). The C<sup>18</sup>O and C<sup>17</sup>O lines have an average value of  $\langle V_{\text{lsr}} \rangle = -6.9 \pm 0.3 \text{ km s}^{-1}$ , and the HCO<sup>+</sup> and H<sup>13</sup>CO<sup>+</sup> lines have a value  $\langle V_{\text{lsr}} \rangle = -7.4 \pm 0.3 \text{ km s}^{-1}$ , while the N<sub>2</sub>H<sup>+</sup> lines seem to have a slightly higher value of  $\langle V_{\text{lsr}} \rangle = -8.1 \pm 0.3 \text{ km s}^{-1}$ . These trends are shown in Figure 5, which is a plot of the velocity and the FWHM, as a function of the upper level energy ( $E_{\text{up}}$ ) for all the spectral line transitions. Taking into account all of the detected lines, we obtain  $\langle V_{\text{lsr}} \rangle = -7.3 \pm 0.5 \text{ km s}^{-1}$ . As a reference, we include in Figure 5 the ammonia observations reported by Beuther et al. (2007) associated to the I-SMA1 and I-SMA2 sources.

In terms of the line width, the HCO<sup>+</sup> lines are somewhat broader than the C<sup>18</sup>O and N<sub>2</sub>H<sup>+</sup> lines, and the C<sup>17</sup>O lines seem to be divided between these two regimes (see Fig. 5). The broadening of the HCO<sup>+</sup> lines, when compared to N<sub>2</sub>H<sup>+</sup>, is consistent with HCO<sup>+</sup> being optically thick, whereas N<sub>2</sub>H<sup>+</sup> is an optically

**Table 1.** Line parameters.

Spectral Line	Frequency [GHz]	HPBW [ $''$ ]	$\eta_{\text{mb}}$	$V_{\text{lsr}}$ [km s $^{-1}$ ]	$T_{\text{peak}}$ [K]	FWHM [km s $^{-1}$ ]	$\int T_{\text{mb}} dV$ [K km s $^{-1}$ ]
C $^{18}$ O(5 – 4)	548.8437	39.5	0.76	$-6.93 \pm 0.01$	$10.3 \pm 0.1$	$5.00 \pm 0.01$	$55.0 \pm 8$
C $^{18}$ O(6 – 5)	658.5683	32.4	0.75	$-6.84 \pm 0.01$	$9.1 \pm 0.1$	$4.93 \pm 0.01$	$48.0 \pm 8$
C $^{18}$ O(7 – 6)	768.2687	27.8	0.75	$-6.67 \pm 0.03$	$7.2 \pm 0.3$	$5.00 \pm 0.06$	$38.4 \pm 6$
C $^{18}$ O(8 – 7)	877.9416	24.4	0.75	$-6.70 \pm 0.01$	$4.9 \pm 0.1$	$4.78 \pm 0.03$	$25.1 \pm 4$
C $^{18}$ O(9 – 8)	987.5840	21.5	0.72	$-7.16 \pm 0.04$	$3.4 \pm 0.2$	$5.40 \pm 0.1$	$19.4 \pm 3$
C $^{18}$ O(10 – 9)	1097.1885	19.4	0.65	$-7.02 \pm 0.06$	$2.5 \pm 0.2$	$4.68 \pm 0.1$	$12.3 \pm 2$
C $^{18}$ O(11 – 10)	1206.7538	17.7	0.66	$-7.02 \pm 0.3$	$1.8 \pm 0.4$	$3.05 \pm 0.6$	$5.7 \pm 1$
C $^{17}$ O(5 – 4)	561.7251	38.6	0.75	$-6.56 \pm 0.01$	$4.3 \pm 0.1$	$4.64 \pm 0.03$	$21.0 \pm 3$
C $^{17}$ O(6 – 5)	674.0249	31.8	0.75	$-6.97 \pm 0.02$	$3.2 \pm 0.1$	$5.28 \pm 0.06$	$17.9 \pm 3$
C $^{17}$ O(7 – 6)	786.3005	27.1	0.75	$-7.55 \pm 0.04$	$2.5 \pm 0.1$	$6.40 \pm 0.1$	$16.7 \pm 3$
C $^{17}$ O(8 – 7)	898.5431	23.8	0.74	$-6.77 \pm 0.06$	$1.6 \pm 0.1$	$4.92 \pm 0.2$	$8.4 \pm 1$
C $^{17}$ O(9 – 8)	1010.7540	21.1	0.71	$-6.67 \pm 0.3$	$1.3 \pm 0.2$	$6.41 \pm 0.03$	$8.8 \pm 1$
HCO $^+$ (6 – 5)	535.0745	40.4	0.76	$-7.25 \pm 0.02$	$8.3 \pm 0.1$	$6.10 \pm 0.01$	$53.8 \pm 8$
HCO $^+$ (7 – 6)	624.2232	34.3	0.75	$-7.16 \pm 0.03$	$6.9 \pm 0.2$	$6.00 \pm 0.07$	$44.2 \pm 7$
HCO $^+$ (8 – 7)	713.3584	30.1	0.75	$-7.22 \pm 0.02$	$4.1 \pm 0.1$	$6.73 \pm 0.05$	$29.6 \pm 4$
HCO $^+$ (9 – 8)	802.4776	26.4	0.75	$-7.24 \pm 0.07$	$2.7 \pm 0.2$	$6.45 \pm 0.2$	$18.7 \pm 3$
HCO $^+$ (10 – 9)	891.5792	24.0	0.74	$-7.36 \pm 0.04$	$2.4 \pm 0.1$	$6.92 \pm 0.09$	$17.5 \pm 3$
HCO $^+$ (11 – 10)	980.6622	21.7	0.73	$-7.86 \pm 0.08$	$1.8 \pm 0.1$	$6.20 \pm 0.2$	$12.0 \pm 2$
HCO $^+$ (12 – 11)	1069.7219	19.9	0.67	$-7.82 \pm 0.2$	$1.3 \pm 0.2$	$5.94 \pm 0.4$	$8.5 \pm 1$
H $^{13}$ CO $^+$ (6 – 5)	520.4728	41.5	0.76	$-7.44 \pm 0.04$	$0.5 \pm 0.1$	$6.44 \pm 0.1$	$3.3 \pm 0.5$
H $^{13}$ CO $^+$ (7 – 6)	607.1893	35.5	0.75	$-7.26 \pm 0.1$	$0.4 \pm 0.1$	$4.17 \pm 0.3$	$1.6 \pm 0.3$
H $^{13}$ CO $^+$ (8 – 7)	693.8924	30.9	0.75	$-6.98 \pm 0.3$	$0.2 \pm 0.1$	$3.04 \pm 0.6$	$0.6 \pm 0.1$
N $_2$ H $^+$ (6 – 5)	558.9808	38.8	0.76	$-7.69 \pm 0.06$	$3.3 \pm 0.2$	$4.58 \pm 0.1$	$16.3 \pm 3$
N $_2$ H $^+$ (7 – 6)	652.1131	32.7	0.75	$-8.07 \pm 0.04$	$1.6 \pm 0.1$	$4.76 \pm 0.09$	$8.3 \pm 1$
N $_2$ H $^+$ (8 – 7)	745.2301	28.8	0.75	$-8.15 \pm 0.09$	$0.9 \pm 0.1$	$4.30 \pm 0.2$	$4.0 \pm 0.6$
N $_2$ H $^+$ (9 – 8)	838.3306	25.5	0.75	$-8.36 \pm 0.3$	$0.4 \pm 0.1$	$4.37 \pm 0.6$	$1.7 \pm 0.3$

**Notes.** For each transition, we report the half-power beamwidth (HPBW), main beam efficiency ( $\eta_{\text{mb}}$ ), LSR velocity ( $V_{\text{lsr}}$ ), peak intensity ( $T_{\text{peak}}$ ), full-width half-maximum (FWHM), and integrated intensity ( $\int T_{\text{mb}} dV$ ). All temperature values are in units of  $T_{\text{mb}}$  [K]. The peak intensity error only includes the statistical error. The integrated intensity error includes the statistical and calibration errors.

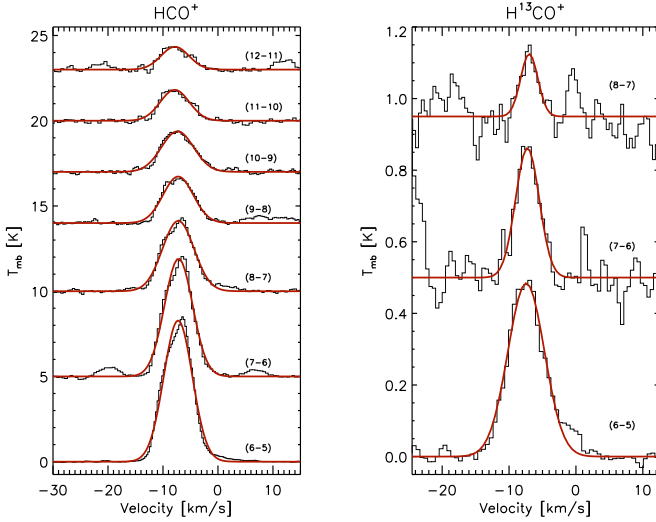


**Fig. 3.** Spectra of the HCO $^+$  and H $^{13}$ CO $^+$  lines. The red lines show the Gaussian fits to the spectra.

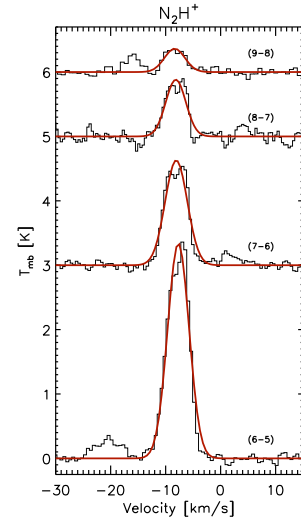


**Fig. 4.** Spectra of the N $_2$ H $^+$  lines. The red lines show the Gaussian fits to the spectra.

thin tracer. The spread in the C $^{17}$ O line widths can be attributed to line contamination from other molecules, such as methanol (CH $_3$ OH) and dimethyl ether (CH $_3$ OCH $_3$ ), present in the C $^{17}$ O spectra. The presence of methanol can also explain some of the spectral features visible in the HCO $^+$  spectra (see HCO $^+$ (7 – 6) spectrum in Fig. 3, for example). There is a spread between the H $^{13}$ CO $^+$  lines that produces a larger uncertainty in the average values, which is probably due to the low signal-to-noise ratio

(SNR) in the H $^{13}$ CO $^+$  spectra, particularly in the (7 – 6) and (8 – 7) transitions. The H $^{13}$ CO $^+$ (6 – 5) spectrum has the best SNR, and its FWHM is consistent with the line widths obtained from the HCO $^+$  lines. For the HCO $^+$  lines we have an average value of  $\langle \text{FWHM} \rangle = 6.3 \pm 0.4$  km s $^{-1}$ , for the C $^{17}$ O lines the  $\langle \text{FWHM} \rangle = 5.5 \pm 0.8$  km s $^{-1}$ , and for the C $^{18}$ O, N $_2$ H $^+$ , and H $^{13}$ CO $^+$  lines we have, respectively,  $\langle \text{FWHM} \rangle = 4.7 \pm 0.8$  km s $^{-1}$ ,  $4.5 \pm 0.2$  km s $^{-1}$ , and  $4.6 \pm 1.7$  km s $^{-1}$ . Taking into account

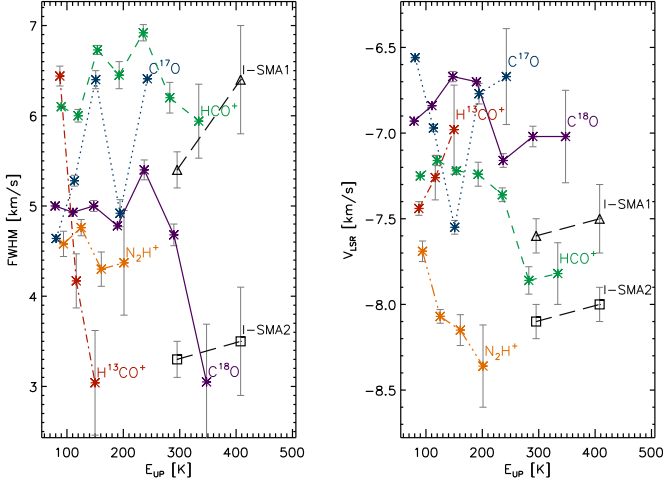


**Fig. 5.** FWHM (left panel) and velocity (right panel) vs. upper level energy  $E_{up}$ , for each of the molecular tracers. The  $\text{NH}_3(5,5)$  and  $(6,6)$  observations reported by Beuther et al. (2007) for I-SMA1 (triangles) and I-SMA2 (squares) are plotted as reference.

all the lines, we obtain  $\langle \text{FWHM} \rangle = 5.0 \pm 1.1 \text{ km s}^{-1}$ . The average values obtained from our observations are in agreement, within the uncertainties, with the values obtained from the  $\text{NH}_3(5,5)$  and  $(6,6)$  observations by Beuther et al. (2007). In particular, the observed  $V_{\text{lsr}}$  and FWHM values seem to agree more with the parameters of the I-SMA1 source than with those of I-SMA2. But given that only two  $\text{NH}_3$  transitions are available, and these occur at slightly higher energies compared to the other molecular transitions (see Fig. 5), we cannot reach definitive conclusions. In addition, the velocities ( $V_{\text{lsr}} = -7.7$  and  $-7.6 \text{ km s}^{-1}$ ) and line widths ( $\text{FWHM} = 5.3$  and  $5.1 \text{ km s}^{-1}$ ) obtained from the APEX observations (Rolfes et al. 2011) for the  $\text{C}^{18}\text{O}(6-5)$  and  $(8-7)$  transitions agree rather well with our results.

In order to search for molecular outflows, we looked for the presence of line-wing emission in the spectra and also in their residuals. Since the  $\text{C}^{18}\text{O}$  and  $\text{HCO}^+$  lines are the most intense transitions, and they do not have a hyperfine structure, they are the best candidates to search for outflows. We found that the line-wing emission seems to be very minor, and is most evident in the  $\text{C}^{18}\text{O}(6-5)$  and  $\text{HCO}^+(6-5)$  transitions, as shown in Figure 6. In particular, the line-wing emission in the  $\text{HCO}^+(6-5)$  transition is only seen in the red-shifted side of the spectra. Line-wing emission is also present in the  $\text{C}^{18}\text{O}(5-4)$  and  $\text{HCO}^+(8-7)$  transitions. In the higher- $J$  transitions, either there is no line-wing emission, or it is less evident than in the lower- $J$  transitions.

## 5. Discussion

### 5.1. Line profiles and kinematical components

The spectral line profiles (Figs. 2 – 4) for the lower-energy transitions of  $\text{C}^{18}\text{O}$ ,  $\text{C}^{17}\text{O}$ ,  $\text{HCO}^+$ , and  $\text{N}_2\text{H}^+$  are asymmetric, with the redshifted side of the profile being stronger than the blueshifted side. This red asymmetry is consistent with emission from optically thick lines from expanding gas. Note that the asymmetry is not seen in the optically thin  $\text{H}^{13}\text{CO}^+$  spectra, and is much less evident in the higher-energy transitions of the other molecules. Although it may be just a fortuitous case, the simultaneous presence of the asymmetry in the optically thick lines and absence in the optically thin lines is a strong evidence

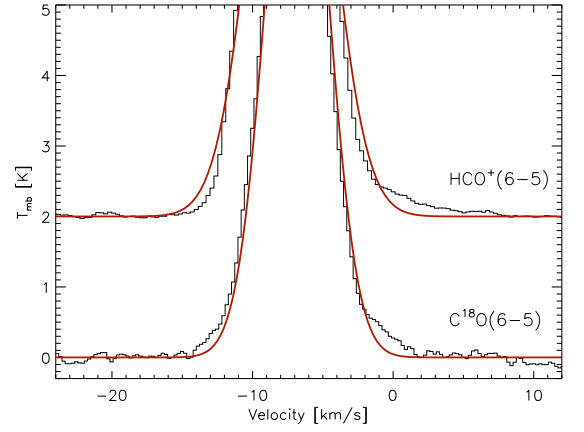


**Fig. 6.** Zoom in on the line-wing emission for the  $\text{C}^{18}\text{O}(6-5)$  and  $\text{HCO}^+(6-5)$  transitions. The red lines show the Gaussian fits to the spectra.

for the presence of an expanding motion of the emitting gas (Mardones et al. 1997).

In the following, we present a quantitative analysis of the line profile in support of the expanding gas hypothesis. As mentioned above, in most cases, a single Gaussian does not fit the observations properly. We attempted to improve the analysis by using a double Gaussian fit in order to decompose the spectra into two kinematical components, which can be justified by the presence of two different velocity components in the line profile. Based on our analysis, and also on the results from previous observations toward NGC 6334 I, we initially assigned a velocity of  $-6.6 \text{ km s}^{-1}$  to the emission from the envelope, and a velocity of  $-9.8 \text{ km s}^{-1}$  to the emission from the core. However, this fit was not unique, as demonstrated by an *a posteriori* analysis of the spectra, in which we used the results from our radiative transfer analysis (Sect. 5.2) as input parameters for a two-component Gaussian model. In particular, the line intensity ratio between the two components obtained from the LVG model indicates that, if the line profile is decomposed into two velocity components, the emission from the core cannot be resolved. In other words, neither of the kinematical components corresponds to emission coming solely from the core. We thus conclude that what we detect in the spectra is a velocity gradient in the emission coming from the envelope of NGC 6334 I. This velocity gradient can effectively explain the redshifted asymmetric profiles and the presence of two kinematical components in the spectra, which can also lead to the conclusion that we are detecting an expansion of the envelope surrounding the hot core of NGC 6334 I. The hypothesis of an expanding gas structure will be further discussed in Section 5.3.

As an example, we show in Figure 7 the double Gaussian profile for the  $\text{C}^{18}\text{O}$  spectra. We have assigned, for the outer and inner envelope emission respectively, velocities of  $-6.0$  and  $-7.5 \text{ km s}^{-1}$ , line widths of  $4.0$  and  $4.7 \text{ km s}^{-1}$ , and the line intensity ratios between the two components are the ones derived from the radiative transfer analysis. Given that for the radiative transfer analysis we are mainly interested in the total emission from the spectra, and that the two-component Gaussian model cannot yet reproduce the line profiles accurately, the results from the single Gaussian profile are the most appropriate to perform the radiative transfer analysis.



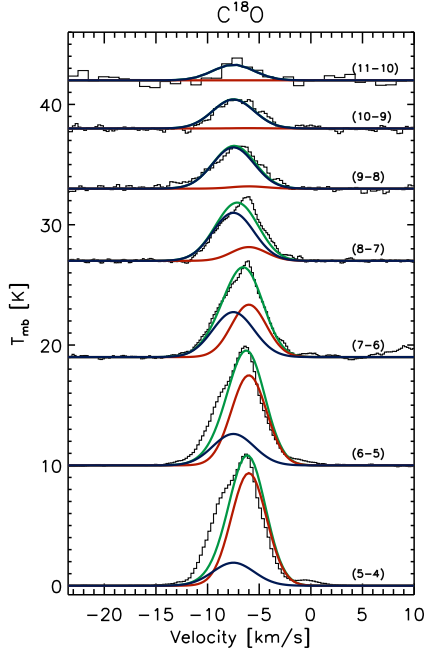


**Fig. 7.** An example of the  $\text{C}^{18}\text{O}$  spectra, overlaid with the double Gaussian profile derived from the results of the LVG analysis. The red, blue, and green lines show, respectively, the Gaussian profiles for the outer and inner envelope emission, and the sum of the two components.

## 5.2. Non-LTE analysis

With the results obtained from the Gaussian fits (Table 1), and using a non-LTE Large Velocity Gradient (LVG) radiative transfer code (Ceccarelli *et al.* 2003), we model the spectral line emission of the observed transitions in order to obtain estimates of the temperature,  $\text{H}_2$  density, size, and CO,  $\text{HCO}^+$  and  $\text{N}_2\text{H}^+$  column density in NGC 6334 I. We achieve this by comparing the observations with the LVG predictions and obtaining a best-fit model by  $\chi^2$  optimization. The optimization is done by first finding the best  $\chi^2$  value for each input value of column density, minimizing it with respect to the other model parameters (i.e., temperature, molecular hydrogen density, and source size). Afterwards, the minimum  $\chi^2$  obtained from the set of column densities corresponds to the model that best fits our results. The uncertainties of the best-fit model are estimated by considering the variation in the resulting parameters for all solutions with  $\chi^2 \leq 0.9$ . The non-LTE LVG code makes use of the collisional coefficients calculated by Flower (1999) for  $\text{HCO}^+$  and  $\text{N}_2\text{H}^+$ . We note that Flower (1999) reports calculations of the  $\text{HCO}^+$ –para- $\text{H}_2$  system for the first 21 energy levels in the temperature range  $5 \leq T \leq 390$  K. In our analysis, we also used the same coefficients for  $\text{N}_2\text{H}^+$  and assumed an ortho- to para- $\text{H}_2$  ratio equal to 0.01, meaning that all  $\text{H}_2$  molecules are in the para state. The collisional coefficients have been retrieved from the BASECOL database<sup>1</sup> (Dubernet *et al.* 2013).

The rotational transitions of  $\text{HCO}^+$ ,  $\text{H}^{13}\text{CO}^+$ ,  $\text{N}_2\text{H}^+$ , and the CO isotopologues all have similar upper level energies and, with the exception of the CO isotopologues, they all have similar critical densities as well. All these transitions are thus likely to probe the same volume of gas within the observed region. Therefore, we wanted to find the model that best fits all the molecular transi-

**Table 2.** Results of LVG analysis.

	Outer envelope	Inner envelope
$n_{\text{H}_2}$ [ $\text{cm}^{-3}$ ]	$(1 \pm 1) \times 10^5$	$(1 \pm 0.5) \times 10^6$
$T$ [K]	$35 \pm 6$	$60 \pm 7$
$\theta$ ["]	$40 \pm 9$	$9 \pm 2$
$r$ [AU]	$(3.4 \pm 0.8) \times 10^4$	$(7.6 \pm 2) \times 10^3$
$N[\text{C}^{18}\text{O}]$ [ $\text{cm}^{-2}$ ]	$(6 \pm 2) \times 10^{16}$	$(2 \pm 3) \times 10^{17}$
$N[\text{HCO}^+]$ [ $\text{cm}^{-2}$ ]	$(3 \pm 2) \times 10^{15}$	$(7 \pm 2) \times 10^{15}$
$N[\text{N}_2\text{H}^+]$ [ $\text{cm}^{-2}$ ]	$(5 \pm 3) \times 10^{14}$	$(3 \pm 1) \times 10^{14}$

**Notes.** For each component, we report the  $\text{H}_2$  density ( $n$ ), temperature ( $T$ ), angular size ( $\theta$ ), linear radius ( $r$ ), and molecular column densities ( $N$ ).

tions simultaneously. To achieve this, we first fitted the  $\text{C}^{18}\text{O}$  and  $\text{C}^{17}\text{O}$  spectral line emission by  $\chi^2$  optimization. Both isotopologues were fitted simultaneously, thus imposing stronger constraints on the model parameters. In practice, a one-component model could not fit the observations properly, indicating that there are indeed two physical components with different physical conditions along the line of sight (Sect. 5.1). We therefore fitted the observations with a two-component model: *a posteriori*, the two components correspond to two regions of the envelope (see Sect. 5.3). Afterwards, the  $\text{HCO}^+$  and  $\text{H}^{13}\text{CO}^+$  spectral line emission were fitted simultaneously, using the  $\text{H}_2$  density, temperature, and source size parameters derived from the CO model as input values and adjusting only the molecular column density in order to obtain the best fit. This last step was repeated for the  $\text{N}_2\text{H}^+$  spectral line emission, so at the end all molecular transitions were fitted with a two-component LVG model, in which the  $\text{C}^{18}\text{O}$ ,  $\text{HCO}^+$  and  $\text{N}_2\text{H}^+$  column densities were the only varying parameter. The results from this method are presented in Table 2 and Figure 8.

We note that the  $\text{C}^{17}\text{O}(8-7)$  transition was excluded from the LVG analysis because it was contaminated by  $\text{CH}_3\text{OH}$  and  $\text{CH}_3\text{OCH}_3$  emission. In addition, given the small number of detected  $\text{N}_2\text{H}^+$  transitions, a one-component model could have been used to fit these observations. But since the two-component model was obtained using a larger data set which could not be fitted by a one-component model, it is more reliable, and therefore it was also used to constrain the model for the  $\text{N}_2\text{H}^+$  emission.

## 5.3. Origin of the emission: the expanding envelope

The radial profiles of density and temperature for NGC 6334 I, obtained by using the specific parameters from the analysis of R11 (Sect. 2), are presented in Figure 9. The parameters obtained from our LVG analysis (Table 2) are overlaid on the profiles in order to compare the two methods. The outer and inner envelope angular radii obtained from the LVG analysis, which are also shown in Fig. 9, correspond to a density and temperature of  $\sim 9 \times 10^4 \text{ cm}^{-3}$  and 38 K for the outer region, and  $\sim 9 \times 10^5 \text{ cm}^{-3}$  and 72 K for the inner region. The results from our analysis are thus remarkably consistent with the radial structure modeled by R11 for NGC 6334 I. As already mentioned in Section 2, the interferometric observations from SMA (Hunter *et al.* 2006) revealed that the hot core of NGC 6334 I is composed of various compact condensations within an angular size of  $\approx 10''$ . Although the *Herschel*/HIFI observations cannot resolve the spatial structure of the hot core, the high level of agreement between the results from our LVG analysis and the results from the radial structure of R11, lead us to the conclusion that our spectral lines include the emission from the envelope of

<sup>1</sup> <http://basecol.obspm.fr/>

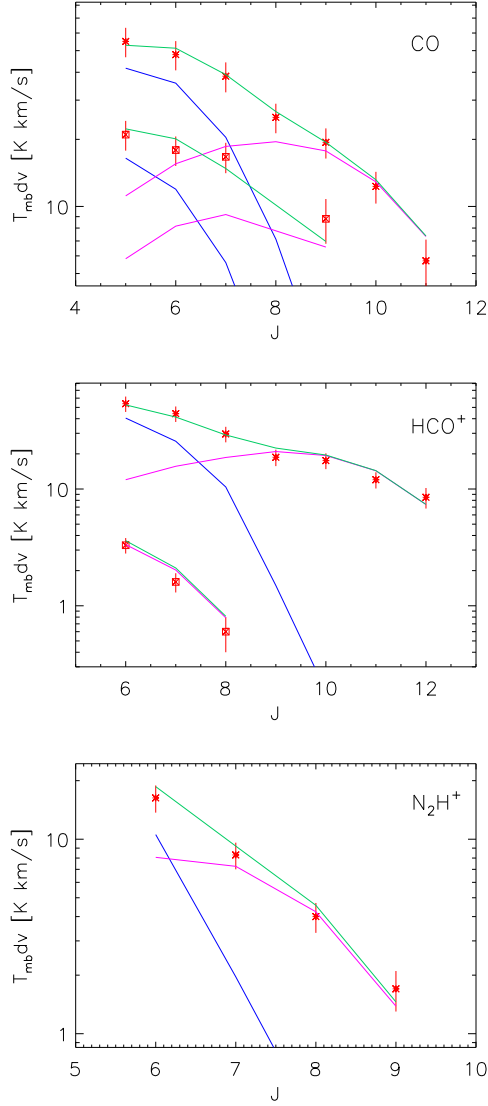


**Fig. 8.** Plots of integrated intensity vs.  $J_{up}$  (from top to bottom) for the C<sup>18</sup>O (red stars) and C<sup>17</sup>O (red squares), HCO<sup>+</sup> (stars) and H<sup>13</sup>CO<sup>+</sup> (squares), and N<sub>2</sub>H<sup>+</sup> (stars) spectral line emission, obtained from the LVG model. The blue and pink lines represent, respectively, the theoretical model for the outer and inner envelope components, and the green lines represent the sum of the two components.

NGC 6334 I. In addition, as mentioned in the Section 5.1, the red asymmetry displayed in the spectra is consistent with expanding gas, and that the Gaussian fits to the line profiles suggested a velocity gradient in the envelope. The LVG analysis confirms that there are indeed two kinematical components in the spectra, with velocities of -6.0 and -7.5 km s<sup>-1</sup>, corresponding to emission from the outer and inner envelope. Based on all this information we conclude that with *Herschel*/HIFI we detect an expansion of the envelope surrounding the hot core of NGC 6334 I, for which we have estimated an expansion velocity of 1.5 km s<sup>-1</sup> over a distance of  $2.6 \times 10^4$  AU (0.13 pc). The results are summarized in Figure 10, which is a representation of the expanding envelope.

Previous studies of giant molecular clouds and HII regions (e.g., Bally & Scoville 1980; Krumholz & Matzner 2009;

Lopez et al. 2011) suggest that, given the expansion velocity and the radial distance at which the expansion is taking place, thermal pressure from hot ionized gas should dominate the envelope expansion in NGC 6334 I. To give an estimate, the flux of ionizing photons produced by the UCHII region associated with NGC 6334 I (de Pree et al. 1995) can exert a thermal pressure,  $P_t/k$ , on the surrounding envelope of  $1.6 \times 10^9$  cm<sup>-3</sup> K. Using our results from the LVG analysis we estimate that the ambient pressure,  $P_a/k$ , exerted by the envelope is between  $10^8$  and  $10^9$  cm<sup>-3</sup> K. Therefore, it is energetically possible to have an envelope expansion in NGC 6334 I. The derived physical parameters for the expanding envelope are further discussed in the following section.

We note that our conclusion of an expanding envelope toward NGC 6334 I is subject to some *caveats*. First, the analysis of the SMA data by Zernickel et al. (2012), as well as the ATCA observations by Beuther et al. (2007) (Sect. 2), indicate a velocity difference between the I-SMA1 and I-SMA2 cores. The emission from these two sources could potentially introduce line asymmetries such as the ones observed in the HIFI spectra. However, we consider this unlikely for the following reasons: (i) the HIFI observations sample gas also at spatial scales which have been filtered out in the SMA maps. Thus, the velocity difference we measure may have a different origin compared to that between I-SMA1 and I-SMA2. (ii) The abundance of molecular ions is expected to be lower toward the very central region of NGC 6334 I, due to the lower CR ionization in such a dense region. Our HCO<sup>+</sup> and N<sub>2</sub>H<sup>+</sup> observations are thus more likely to probe a much larger volume of gas compared to that of the interferometric observations. (iii) The HCO<sup>+</sup> and N<sub>2</sub>H<sup>+</sup> emitting sizes (Table 2) are larger than those measured for the hot cores, while they are consistent with emission from a larger scale, such as that from the envelope. (iv) R11 found infall signature in HCN high-excitation lines, while our HCO<sup>+</sup> line profiles show no signs of infall, which is suggesting that our spectra are mostly sensitive to less dense gas. However, the many observations now becoming available add up to the complexity of this and other similar regions, showing multiple kinematic signatures. Therefore, building a complete picture of the structure of NGC 6334 I will require multi-line interferometric observations with zero-spacing to be sensitive to both core and envelope components.

#### 5.4. The ionization structure of the envelope

##### 5.4.1. Column densities and molecular abundances

Using the results from the LVG analysis we can derive estimates of the H<sub>2</sub> column density, as well as the relative abundances between the various molecular species. With the column densities of HCO<sup>+</sup> and N<sub>2</sub>H<sup>+</sup> listed in Table 2 we obtain an [HCO<sup>+</sup>]/[N<sub>2</sub>H<sup>+</sup>] abundance ratio of 6 and 23 for the outer and inner envelope components, respectively. We derive the CO column densities using an abundance ratio of [CO]/[C<sup>18</sup>O] = 500 (Emprechtinger et al. 2010), and from the H<sub>2</sub> densities and the linear size of the inner and outer envelope we compute the H<sub>2</sub> column densities. Afterwards, we obtain the relative abundances of HCO<sup>+</sup> and N<sub>2</sub>H<sup>+</sup> with respect to CO and H<sub>2</sub>, and the [CO]/[H<sub>2</sub>] abundance ratios. These results are listed in Table 3. As a comparison, we have also listed the H<sub>2</sub> column densities computed using the radial density profile from R11 and the same method described above, which are consistent with our results. We find that in the inner envelope the HCO<sup>+</sup> and CO abundances are higher when compared to the abundances in the outer enve-

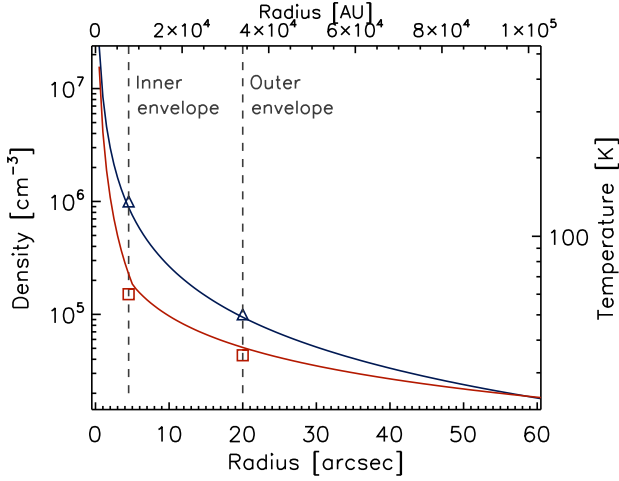


**Fig. 9.** Radial profiles of the density (blue line) and temperature (red line) toward NGC 6334 I from R11. The vertical lines indicate, respectively, the angular radius of the inner and outer regions obtained from our LVG analysis. The density (blue triangles) and temperature (red squares) values obtained for each component are overlaid on the plot.

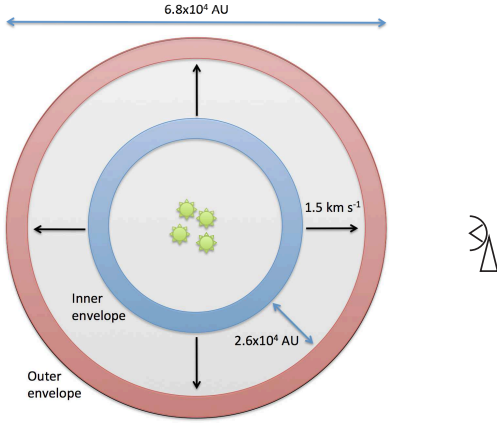


**Fig. 10.** Representation of the expanding envelope toward NGC 6334 I. See Sect. 5.3 for explanation.

lope, while the opposite is true for the  $\text{N}_2\text{H}^+$  abundance. This relationship can be explained by considering the chemical network of these three molecules in which, for  $[\text{CO}]/[\text{H}_2]$  abundances of  $\sim 10^{-4}$ ,  $\text{N}_2\text{H}^+$  is destroyed through reactions with CO, forming  $\text{HCO}^+$  in the process (see Bergin et al. 1997 for a detailed explanation).

For the computation of the CO column densities we assumed, as is common practice, that the  $\text{CO}/\text{C}^{18}\text{O}$  ratio equals the  $^{16}\text{O}/^{18}\text{O}$  ratio. This oxygen isotopic ratio has been estimated for the ISM by Smith et al. (2009) as a function of the source distance from the Galactic center. At a galactocentric distance of 6.8 kpc for NGC 6334 (Kraemer et al. 1998, 2000) we obtain a  $^{16}\text{O}/^{18}\text{O}$  ratio of  $488 \pm 68$  for NGC 6334 I. The variation in the CO column densities due to this slight decrease in the  $^{16}\text{O}/^{18}\text{O}$  ratio is less than 3%, and therefore does not affect our results for the relative abundances.

**Table 3.** Derived parameters.

	Outer envelope	Inner envelope
$\text{N}[\text{H}_2]$ [ $\text{cm}^{-2}$ ] <sup>a</sup>	$10^{23}$	$2 \times 10^{23}$
$[\text{HCO}^+]/[\text{N}_2\text{H}^+]$	6	23
$[\text{CO}]/[\text{H}_2]$	$3 \times 10^{-4}$	$5 \times 10^{-4}$
$[\text{HCO}^+]/[\text{H}_2]$	$3 \times 10^{-8}$	$3.5 \times 10^{-8}$
$[\text{N}_2\text{H}^+]/[\text{H}_2]$	$5 \times 10^{-9}$	$1.5 \times 10^{-9}$
$[\text{HCO}^+]/[\text{CO}]$	$10^{-4}$	$7 \times 10^{-5}$
$[\text{N}_2\text{H}^+]/[\text{CO}]$	$1.7 \times 10^{-5}$	$3 \times 10^{-6}$
$\text{N}[\text{H}_2]$ [ $\text{cm}^{-2}$ ] <sup>b</sup>	$9.6 \times 10^{22}$	$2 \times 10^{23}$
$\zeta_{\text{H}_2}$ [ $\text{s}^{-1}$ ]	$2.0 \times 10^{-16}$	$8.5 \times 10^{-17}$

**Notes.** For each component, we report the  $\text{H}_2$  column density ( $\text{N}$ ), relative abundances, and cosmic ray ionization rate ( $\zeta_{\text{H}_2}$ ). <sup>(a)</sup> Computed using the results of LVG analysis (Sect. 5.4.1). <sup>(b)</sup> Computed using the results of the radial profiles from R11 (Sect. 5.3).

As for the  $[\text{CO}]/[\text{H}_2]$  abundance ratio, we obtained values of  $3 \times 10^{-4}$  and  $5 \times 10^{-4}$  for the outer and inner envelope, which are higher than the “standard” dense cloud value of  $10^{-4}$  (Burgh et al. 2007, and references therein). These abundance ratios were obtained using  $\text{H}_2$  column densities of  $10^{23}$  and  $2 \times 10^{23} \text{ cm}^{-2}$  for the outer and inner envelope respectively, as listed in Table 3. There are two alternative methods to compute the  $\text{H}_2$  column density, in addition to the one previously described.

The first alternative method is to use the derived CO column density and the  $[\text{CO}]/[\text{H}_2]$  standard dense cloud value to compute the  $\text{H}_2$  column density. Using this method we obtain higher column densities by a factor of 3 and 5 for the outer and inner envelope of NGC6334I. The second alternative method is to assume the source has a spherical symmetry and a radial density profile of the form

$$n(r) = \frac{n_0}{1 + (r/R)^{1.5}}, \quad (1)$$

where  $n_0$  and  $R$  are, respectively, the  $\text{H}_2$  density and envelope radius for the outer and inner components. The  $\text{H}_2$  column densities are then computed by integrating this density profile along the line of sight, after a convolution with a 2D Gaussian corresponding to the HIFI beam. Using this method, we obtain  $\text{H}_2$  column densities that are lower by a factor of 1.7 and 2, and  $[\text{CO}]/[\text{H}_2]$  abundance ratios of  $5 \times 10^{-4}$  and  $10^{-3}$ , for the outer and inner envelope. A more detailed radiative transfer analysis, which also takes into account the envelope structure, would be needed to better understand the variations in the column density and  $[\text{CO}]/[\text{H}_2]$  abundance ratio, but this kind of analysis is beyond the scope of the present work.

#### 5.4.2. Chemical modeling

We have modeled the chemical evolution of the source using the gas-phase reaction network from the KInetic Database for Astrochemistry (KIDA) in conjunction with the Nahoon code (Wakelam et al. 2012). The KIDA network contains over 6000 unique chemical reactions involving almost 500 different species and a total of 6467 rate coefficients. The Nahoon code uses this database to compute the chemical evolution at a fixed temperature (between 10 – 300 K), density, and CR ionization rate. The chemical network of  $\text{HCO}^+$  and  $\text{N}_2\text{H}^+$  in dense regions (e.g., Turner 1995; Bergin et al. 1997) is dominated by the CR ionization rate. For this reason, we want to derive an estimate of the CR ionization rate toward the envelope of NGC 6334 I. By running a grid of Nahoon models in a range of  $\text{H}_2$  densities and CR



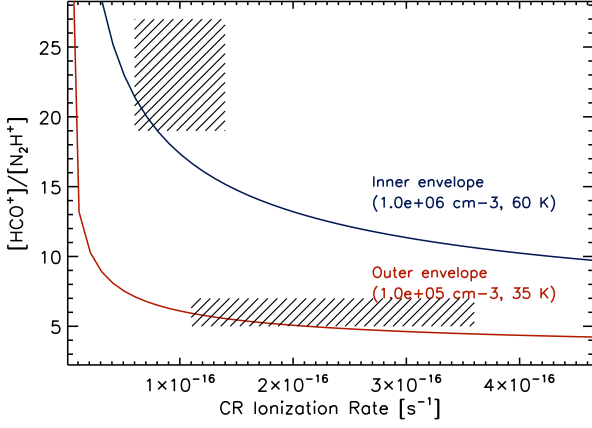


**Fig. 11.**  $[\text{HCO}^+]/[\text{N}_2\text{H}^+]$  abundance ratio as a function of the CR ionization rate, computed for the inner (blue line) and outer envelope (red line) components. The rectangles represent the results obtained within a 20% uncertainty interval. See text for discussion.

ionization rates ( $\zeta^{\text{H}_2}$ ), we compute the expected  $[\text{HCO}^+]/[\text{N}_2\text{H}^+]$  abundance ratios for the two temperature components. Through the comparison of the model results with the  $\text{H}_2$  densities and  $[\text{HCO}^+]/[\text{N}_2\text{H}^+]$  abundance ratios derived from the LVG analysis, we then obtain an estimate for  $\zeta^{\text{H}_2}$  toward NGC 6334 I. Afterwards, we run a final Nahoon model in which the  $\text{H}_2$  density and  $\zeta^{\text{H}_2}$  are fixed using the previously obtained values, and compute once more the  $[\text{HCO}^+]/[\text{N}_2\text{H}^+]$  abundance ratio for each temperature component. The difference (at the  $\sim 20\%$  level) between the  $[\text{HCO}^+]/[\text{N}_2\text{H}^+]$  abundance ratios obtained from the LVG analysis and the ones obtained with the Nahoon code will be used below to estimate the uncertainty between both models.

Using this method we find values of  $2.0 \times 10^{-16}$  and  $8.5 \times 10^{-17} \text{ s}^{-1}$  for the CR ionization rate in the outer and inner envelope components, respectively. Thus the CR ionization rate in the outer envelope is approximately two times higher than in the inner envelope of NGC 6334 I, and both values are higher than the “standard” CR ionization rate in molecular clouds of  $\zeta^{\text{H}_2} \approx 10^{-17} \text{ s}^{-1}$  (Padovani et al. 2009, and references therein). We note that the values of  $\zeta^{\text{H}_2}$ , and also the  $\text{H}_2$  column densities, obtained for NGC 6334 I are similar to previous values obtained by van der Tak & van Dishoeck (2000) and Doty et al. (2002) toward the envelopes surrounding massive protostellar sources. In Figure 11 we present the computed  $[\text{HCO}^+]/[\text{N}_2\text{H}^+]$  abundance ratio as a function of the CR ionization rate for the outer and inner envelope components, in which the  $\text{H}_2$  densities and temperatures obtained from the LVG analysis have been used as input parameters for the Nahoon model. Overlaid are the ranges of abundance ratios and CR ionization rates obtained for each component when the  $[\text{HCO}^+]/[\text{N}_2\text{H}^+]$  ratio is varied by  $\pm 20\%$  (corresponding to the difference between the LVG and Nahoon results) with respect to the values listed in Table 3.

The fact that the CR ionization rate is higher in the outer envelope than in the inner envelope indicates that the main source of ionization originates outside of NGC 6334 I. It was already mentioned that the ionization in dense regions, like the envelope of NGC 6334 I, is dominated by CRs. But X-ray emission from young massive stars in the surrounding molecular cloud could also contribute as a source of ionization. X-

ray emission in the NGC 6334 giant molecular cloud has been revealed through observations with the *Advanced Satellite for Cosmology and Astrophysics* (ASCA; Sekimoto et al. 2000) and the *Chandra X-Ray Observatory* (Ezoe et al. 2006) in the energy range of 0.5–10 keV. The X-ray emission is mainly associated with young massive stars embedded in the five far-infrared (FIR) regions denoted NGC 6334 I–V. Therefore, the nearest sources of X-rays should be from cores II–V in NGC 6334 and from the interior of NGC 6334 I itself. From the ASCA observations, Sekimoto et al. (2000) obtained X-ray luminosities ( $L_X$ ) and hydrogen column densities ( $N_H$ ) for each of the five cores, and then computed the radius ( $r_X$ ) inside which the X-ray ionization rate ( $\zeta_X$ ) is greater than the standard value for the CR ionization rate using the equation given by Maloney et al. (1996):

$$\zeta_X = 1.4 \times 10^{-18} \text{ s}^{-1} \frac{L_X}{10^{33} \text{ erg s}^{-1}} \frac{1 \text{ pc}^2}{r_X^2} \frac{10^{22} \text{ cm}^{-2}}{N_H} \quad (2)$$

With X-ray luminosities of  $\sim 10^{33} \text{ erg s}^{-1}$  and column densities of  $\sim 10^{22} \text{ cm}^{-2}$  for each of the five cores, and assuming  $\zeta_X = 10^{-17} \text{ s}^{-1}$ , Sekimoto and co-authors determined that the X-ray ionization rate is comparable to that by cosmic rays within a radius of  $\sim 0.3 \text{ pc}$  from each core. This distance is much less than the distance between cores II–V and core I, and therefore there should be no significant ionization in NGC 6334 I due to external X-ray sources. As for the X-ray emission from the interior of NGC 6334 I, the authors obtained  $L_X = 0.66 \times 10^{33} \text{ erg s}^{-1}$  and  $N_H = 2.0 \times 10^{22} \text{ cm}^{-2}$ . By using equation (2) with our  $\zeta^{\text{H}_2}$  values from Table 3, we obtain that for the outer envelope ( $r = 0.16 \text{ pc}$ ) X-ray ionization is significant up to a radius of 0.05 pc. The ionization in the outer envelope should thus be dominated by cosmic rays. However for the inner envelope ( $r = 0.04 \text{ pc}$ ) X-ray ionization is significant up to a radius of 0.07 pc. Therefore the cosmic ray ionization rate value for the inner envelope should be treated as an upper limit due to any additional contribution from X-ray emission.

As a final exercise, we computed the theoretical value of the CR ionization rate as a function of the column density of traversed matter for NGC 6334 I using the models from Padovani et al. (2009). The models include a detailed treatment of CR propagation, taking into account the decrease of the ionization rate as the incident CRs penetrate the cloud. Using the  $\text{N}[\text{H}_2]$  column densities in Table 3 we obtain CR ionization rates of  $1.4 \times 10^{-16}$  and  $9.5 \times 10^{-17} \text{ s}^{-1}$  for the outer and inner envelope components, respectively. These values are well within the uncertainties of the values obtained from the KIDA/Nahoon chemical model (Table 3 and Fig. 11) which, given the differences between the two methods used to estimate the CR ionization rate, can be indicative of the strength of the analysis.

## 6. Summary and conclusions

We presented high-resolution spectral line observations of the high-mass star-forming region NGC 6334 I obtained with the HIFI instrument on board *Herschel*. In total, five molecular species were analyzed through several rotational transitions with  $J_{\text{up}} \geq 5$ . The results of our study can be summarized as follows:

1. We detected bright emission from the  $\text{HCO}^+$  and  $\text{N}_2\text{H}^+$  molecular ions, which allow us to constrain the ionization in the warm and dense regions of NGC 6334 I.
2. Optically thick  $\text{HCO}^+$  and  $\text{N}_2\text{H}^+$  lines display profiles with a redshifted asymmetry, while optically thin  $\text{H}^{13}\text{CO}^+$  lines have a Gaussian profile peaked at the absorption dip of the optically thick lines. This is evidence of an expanding gas.

3. A non-LTE LVG radiative transfer analysis of the integrated line intensities shows the presence of two physical components, whose temperatures and densities are consistent with those previously derived for the outer and inner envelope of NGC 6334 I respectively.
4. The envelope surrounding the hot core of NGC 6334 I is expanding at a velocity of  $1.5 \text{ km s}^{-1}$  over a distance of  $2.6 \times 10^4 \text{ AU}$ . Thermal pressure from hot ionized gas can provide the driving force required for the envelope expansion.
5. The  $\text{HCO}^+$  and CO abundances are higher in the inner envelope than in the outer envelope, and the opposite is true for the  $\text{N}_2\text{H}^+$  abundance. The  $[\text{CO}]/[\text{H}_2]$  abundance ratio varies from  $3 \times 10^{-4}$  to  $5 \times 10^{-4}$  between the outer and inner envelope, which is higher than the “standard” dense cloud value of  $10^{-4}$ .
6. The CR ionization rate in the outer envelope ( $2 \times 10^{-16} \text{ s}^{-1}$ ) is higher than in the inner envelope ( $\sim 9 \times 10^{-17} \text{ s}^{-1}$ ) by a factor of approximately 2, indicating that the main source of ionization lies outside NGC 6334 I. The ionization in the outer envelope is likely dominated by CRs, but there could be an additional contribution to the ionization in the inner envelope from X-ray emission originating in the interior of NGC 6334 I.
7. The values obtained for the CR ionization rate are consistent, within the errors, with previous models that compute the CR ionization rate through a detailed treatment of CR propagation in molecular clouds, and they are also similar to previous values obtained toward the envelopes surrounding massive protostellar sources.

**Acknowledgements.** HIFI has been designed and built by a consortium of institutes and university departments from across Europe, Canada and the United States under the leadership of SRON Netherlands Institute for Space Research, Groningen, The Netherlands and with major contributions from Germany, France and the US. Consortium members are: Canada: CSA, UWaterloo; France: CESR, LAB, LERMA, IRAM; Germany: KOSMA, MPIfR, MPS; Ireland, NUI Maynooth; Italy: ASI, IFSI-INAf, Osservatorio Astrofisico di Arcetri-INAf; Netherlands: SRON, TUD; Poland: CAMK, CBK; Spain: Observatorio Astronómico Nacional (IGN), Centro de Astrobiología (CSIC-INTA). Sweden: Chalmers University of Technology - MC2, RSS & GARD; Onsala Space Observatory; Swedish National Space Board, Stockholm University - Stockholm Observatory; Switzerland: ETH Zurich, FHNW; USA: Caltech, JPL, NHSC. Support for this work was provided by NASA through an award issued by JPL/Caltech. JMO acknowledges the support of NASA, through the PR NASA Space Grant Doctoral Fellowship, and from the Institut de Planétologie et d’Astrophysique de Grenoble (IPAG). C.Ceccarelli acknowledges the financial support from the French Agence Nationale pour la Recherche (ANR) (project FORCOMS, contract ANR-08-BLAN-0225) and the French spatial agency CNES. The authors also wish to thank Marco Padovani for providing the fit models for the CR ionization rate, Alexander Zernickel for providing the map of NGC 6334 I, and Ana López-Sepulcre, whose comments contributed to improve this work.

## References

- Balbus, S. A. & Hawley, J. F. 1998, *Reviews of Modern Physics*, 70, 1
- Bally, J. & Scoville, N. Z. 1980, *ApJ*, 239, 121
- Bergin, E. A., Goldsmith, P. F., Snell, R. L., & Langer, W. D. 1997, *ApJ*, 482, 285
- Beuther, H., Thorwirth, S., Zhang, Q., et al. 2005, *ApJ*, 627, 834
- Beuther, H., Walsh, A. J., Thorwirth, S., et al. 2007, *A&A*, 466, 989
- Brooks, K. J. & Whiteoak, J. B. 2001, *MNRAS*, 320, 465
- Burgh, E. B., France, K., & McCandliss, S. R. 2007, *ApJ*, 658, 446
- Ceccarelli, C., Bacmann, A., Boogert, A., et al. 2010, *A&A*, 521, L22
- Ceccarelli, C., Hily-Blant, P., Montmerle, T., et al. 2011, *ApJ*, 740, L4
- Ceccarelli, C., Maret, S., Tielens, A. G. G. M., Castets, A., & Caux, E. 2003, *A&A*, 410, 587
- Cesaroni, R. 2005, in *IAU Symposium*, Vol. 227, *Massive Star Birth: A Crossroads of Astrophysics*, ed. R. Cesaroni, M. Felli, E. Churchwell, & M. Walmsley, 59–69
- Codella, C., Lefloch, B., Ceccarelli, C., et al. 2010, *A&A*, 518, L112
- Comito, C. & Schilke, P. 2002, *A&A*, 395, 357
- de Pree, C. G., Rodriguez, L. F., Dickel, H. R., & Goss, W. M. 1995, *ApJ*, 447, 220
- Doty, S. D., van Dishoeck, E. F., van der Tak, F. F. S., & Boonman, A. M. S. 2002, *A&A*, 389, 446
- Dubernet, M.-L., Alexander, M. H., Ba, Y. A., et al. 2013, *A&A*, 553, A50
- Emprechtinger, M., Lis, D. C., Bell, T., et al. 2010, *A&A*, 521, L28
- Emprechtinger, M., Lis, D. C., Rolfs, R., et al. 2013, *ApJ*, 765, 61
- Ezoe, Y., Kokubun, M., Makishima, K., Sekimoto, Y., & Matsuzaki, K. 2006, *ApJ*, 638, 860
- Flower, D. R. 1999, *MNRAS*, 305, 651
- Gammie, C. F. 1996, *ApJ*, 457, 355
- Hunter, T. R., Brogan, C. L., Megeath, S. T., et al. 2006, *ApJ*, 649, 888
- Kraemer, K. E., Jackson, J. M., & Lane, A. P. 1998, *ApJ*, 503, 785
- Kraemer, K. E., Jackson, J. M., Lane, A. P., & Paglione, T. A. D. 2000, *ApJ*, 542, 946
- Krumholz, M. R. & Matzner, C. D. 2009, *ApJ*, 703, 1352
- Langer, W. D. & Penzias, A. A. 1990, *ApJ*, 357, 477
- Lis, D. C., Pearson, J. C., Neufeld, D. A., et al. 2010, *A&A*, 521, L9
- Lopez, L. A., Krumholz, M. R., Bolatto, A. D., Prochaska, J. X., & Ramirez-Ruiz, E. 2011, *ApJ*, 731, 91
- Maloney, P. R., Hollenbach, D. J., & Tielens, A. G. G. M. 1996, *ApJ*, 466, 561
- Mardones, D., Myers, P. C., Tafalla, M., et al. 1997, *ApJ*, 489, 719
- Miettinen, O., Harju, J., Haikala, L. K., & Juvela, M. 2012, *A&A*, 538, A137
- Migenes, V., Horiuchi, S., Slysh, V. I., et al. 1999, *ApJS*, 123, 487
- Neckel, T. 1978, *A&A*, 69, 51
- Ossenkopf, V., Müller, H. S. P., Lis, D. C., et al. 2010, *A&A*, 518, L111
- Ott, S. 2010, in *Astronomical Society of the Pacific Conference Series*, Vol. 434, *Astronomical Data Analysis Software and Systems XIX*, ed. Y. Mizumoto, K.-I. Morita, & M. Ohishi, 139
- Padovani, M., Galli, D., & Glassgold, A. E. 2009, *A&A*, 501, 619
- Padovani, M., Galli, D., & Glassgold, A. E. 2013, *A&A*, 549, C3
- Penzias, A. A. 1981, *ApJ*, 249, 518
- Rivera-Ingraham, A., Martin, P. G., Polychroni, D., et al. 2013, *ApJ*, 766, 85
- Roelfsema, P. R., Helmich, F. P., Teyssier, D., et al. 2012, *A&A*, 537, A17
- Rolfs, R., Schilke, P., Wyrowski, F., et al. 2011, *A&A*, 527, A68
- Sandell, G. 2000, *A&A*, 358, 242
- Sekimoto, Y., Matsuzaki, K., Kamae, T., et al. 2000, *PASJ*, 52, L31
- Smith, R. L., Pontoppidan, K. M., Young, E. D., Morris, M. R., & van Dishoeck, E. F. 2009, *ApJ*, 701, 163
- Turner, B. E. 1995, *ApJ*, 449, 635
- van der Tak, F. F. S. & van Dishoeck, E. F. 2000, *A&A*, 358, L79
- van der Wiel, M. H. D., van der Tak, F. F. S., Lis, D. C., et al. 2010, *A&A*, 521, L43
- Wakelam, V., Herbst, E., Loison, J.-C., et al. 2012, *ApJS*, 199, 21
- Walsh, A. J., Burton, M. G., Hyland, A. R., & Robinson, G. 1998, *MNRAS*, 301, 640
- Walsh, A. J., Longmore, S. N., Thorwirth, S., Urquhart, J. S., & Purcell, C. R. 2007, *MNRAS*, 382, L35
- Zernickel, A., Schilke, P., Schmiedeke, A., et al. 2012, *A&A*, 546, A87
- Zinnecker, H. & Yorke, H. W. 2007, *ARA&A*, 45, 481